ORIGINAL ARTICLE

Experimental investigation of the fracture grouting efficiency with consideration of the viscosity variation under dynamic pressure conditions

Chenghao Han[1] · Weijie Zhang[1,2] · Wenwu Zhou[1] · Jianbin Guo[1,2] · Fei Yang[1] · Xiaoquan Man[1] · Jigang Jiang[1] · Chunrui Zhang[1] · Yongjie Li[1] · Zheng Wang[1] · Hao Wang[1]

Abstract

Grouting techniques have been extensively and effectively implemented to prevent water bursts originating from limestone aquifers in underground mining. Using widely employed grout with time-varying viscosity, promoting the effective propagation of slurry in fractures, especially fractures with narrow apertures, and improving the grouting efficiency (GE) are critical issues that remain unsolved. In this study, an experimental investigation of the fracture GE was conducted considering the dynamically changing injection pressure for viscosity--time-dependent grout using a fracture model constructed from acrylic glass. Three grouting pressure adjustment schemes (periodic-increasing pressure, constant pressure and periodic-reducing pressure) and two narrow hydraulic apertures (200 and 250 μm) were selected for testing. Each trial utilizing the fracture replica was filmed, allowing the advancing slurry to be analyzed versus the propagation distance over time. The measured penetration lengths and fracture GE were then compared with the simulation data. The measured penetration length versus time curves agreed well with the theoretical data. Moreover, the pressure adjustment mode and grout rheology significantly impacted the GE. In general, the periodic increases in pressure reduced the *GE*, which decreased by 4.16% and 10.19% for the slow- and rapid-growth viscosity grouts (G1 and G2), respectively. However, phase reduction of the pressure considerably enhanced the GE. Relative grouting efficiency (*RGE*) was increased by 3.18% and 10.08% for G1 and G2, respectively, indicating that a step-by-step reduction in the injection pressure can effectively improve the GE for the remarkable rheological grout during the grouting process. Additionally, the tests suggested that the hydraulic aperture width has an unclear effect on the GE of microfissures.

Keywords Artificial fracture · Grouting efficiency · Dynamic pressure grouting · Viscosity-time-dependent

Introduction

In China, many water inrush disasters have been encountered in coal mines with the high-intensity mining of coal resources, which have led to significant safety challenges

✉ Weijie Zhang
sduzhangweijie@126.com

[1] College of Earth Science and Engineering, Shandong University of Science and Technology, 579 Qianwangang Road, Huangdao District, Qingdao 266590, Shandong, China

[2] Shandong Provincial Key Laboratory of Depositional Mineralization and Sedimentary Mineral, Shandong University of Science and Technology, Qingdao 266590, China

for underground coal mining (Wu et al. 2011; Cheng et al. 2013; Guo et al. 2017; Yin et al. 2016, 2018, 2019; Zhang et al. 2017a, b; Li et al. 2018a, b, 2019b; Wang and Meng 2018; Shi et al. 2019; Wang et al. 2019). Statistics show that limestone aquifers are one of the most important disaster sources of water bursts in the coal mines of North China, where coal-bearing strata generally develop in the Carboniferous–Permian and overlay an Ordovician karst aquifer with high groundwater pressure and abundant water (Sun et al. 2015; Zeng et al. 2016; Li et al. 2018a, b, 2019a; Wang and Shi 2019). In addition, several karst aquifers developed in the roof and/or floor of the main minable coal seams. Mining-induced cracks are generated and expand during the advancement of the working face, causing the gradual communication with the goaf and the nearby karst aquifer, while the goaf directly connects with the Ordovician aquifer via

a mining-induced fracture or fault in some cases, leading to water inrush (Tan et al. 2010, 2012; Lu and Wang 2015; Guo et al. 2016; Yu et al. 2017; Wang et al. 2017; Huang et al. 2018).

To prevent water ingress, the grouting technique has been extensively and effectively implemented for water-bearing strata or channels in underground mining (Yao et al. 2013; Mohajerani et al. 2015; Zhang et al. 2018). A slurry is poured into the rock fracture, propagates in the karst fissure network and then seals the water conduction channels, thus enhancing the impermeability and strength of the floor (Sui et al. 2015; Sun et al. 2018). However, due to the complex distribution of the fracture networks, unclear geological surveys, and improper engineering operations, improving the grouting efficiency (GE) and reducing the "project cost" (also including energy consumption, the quantity of grouting materials and time) have become critical issues for fracture grouting practices (Wei et al. 2019).

The GE in a fractured rock mass is affected by many factors, such as the aperture width, fracture roughness, grouting control mode, i.e., flow rate grouting and pressure grouting, properties of the grout material, characteristics of the fractures, and effects of the multiphysical fields (Sui et al. 2015). To understand the grouting mechanism of the fractured rock mass, various scholars have carried out considerable research.

The movement of slurry in an ideal fracture has been widely discussed (Littlejohn 1975; Gustafson et al. 1996; Axelsson et al. 2009; Mohammed et al. 2015; Funehag and Thorn 2018). Funehag and Fransson (2006) studied the pressure in the grouting process and obtained the pressure by a short-term pressure grouting test. Funehag and Gustafson (2008a; b) proposed a diffusion formula at a constant grouting pressure for silica sol. Penetration equations in fractures under constant grouting flow rates were also obtained (Dai and Bird 1981; Hassler et al. 1992; Amadei and Savage 2001).

In recent decades, many kinds of grout with time-varying viscosity (e.g., some typical cement-based slurry and chemical materials) have been widely adopted in the fracture grouting process. Many studies have focused on the grouting process with respect to the time-varying slurry viscosity. Li et al. (2013) obtained the time-dependent viscosity function of a cement–sodium grout based on the experimental study. Furthermore, Zhang et al. (2017a, b) studied the grouting mechanism of quick setting slurry in rock fissure considering the spatial variation of viscosity. Zhang et al. (2018) investigated the fracture grouting mechanism with a cement and sodium silicate grout and discussed the factors influencing the propagation length. Mohajerani et al. (2015) proposed the explicit grout forehead pressure (EGFP) algorithm to calculate the penetration length considering the time-varying viscosity of the slurry.

In a field grouting practice, experienced engineers often change the grouting parameters, such as the flow rate, injection pressure or the proportion of slurry composition (in essence, to change the rheological properties of the slurry) in a grouting operation, to promote the propagation of the slurry in a fracture, as verified by in situ tests (Li et al. 2014). This grouting method is called dynamic grouting. Wei et al. (2019) proposed a stepwise algorithm to study the advancing process of grouting with the significant rheological property of the crack with the periodic adjustment of the grouting operation parameters. This theoretical research indicated that, compared with the customary constant parameter grouting, increasing or decreasing the injection pressure or flow rate changes the fracture GE to some extent.

The main objective of this paper is to study the slurry diffusion process and GE of the fracture grouting condition with a periodic adjustment of the grouting pressure via a laboratory investigation. In this study, typical silica sol grouts with different viscosity functions, two hydraulic apertures (200 μm and 250 μm), and three pressure adjustment schemes (phased increased pressure grouting, phased constant pressure grouting, and reduced pressure grouting) were adopted in the experimental design. Then, a series of fracture grouting model tests were conducted. Compared with the theoretical results, the experimental data indicated that the phased increased pressure reduces the fracture GE, whereas the phased reduced pressure significantly improves the GE, especially for the slurry with a high-speed increasing viscosity.

Method

In China, materials used for fracture grouting include cement-based grouts (e.g., cement slurry, cement–sodium silicate slurry) and chemical grouts (e.g., silica sol, urea–formaldehyde resin). Most of the selected materials are marked by the time-varying viscosity, which is also called rheology. In general, the rheological properties of grouts can be changed by adjusting the proportions of their components, significantly impacting their gelling time. This process tends to control the propagation of fracture grouting. Furthermore, a better grouting effect could be produced with the dynamic adjustment of grouting operation parameters, such as the injection pressure or flow rate.

The main objectives of this study are to investigate the GE by considering both the time-varying viscosity of grouts and the adjustment of the grouting operation parameters under hydrostatic conditions. The GE could be expressed as a function of the penetration length, injection pressure, and grouting time (Wei et al. 2019). In our conventional understanding, the GE is considered high if a small consumption of mechanical energy produces a large grouted region

during a fracture grouting process. Therefore, the GE can be defined as the ratio of the maximum penetration length to the consumption of the mechanical energy in a time interval as follows:

$$GE = \frac{r_{max}}{E_g}, \tag{1}$$

where GE is the grouting efficiency, r_{max} is the maximum propagation distance, and E_g is the mechanical energy provided by the grouting equipment to drive slurry diffusion, which can be approximately obtained by integrating the grouting pressure over the injection time according to Eq. (2).

$$E_g = \int_0^{(n-1)dt} p_g(t)dt, \tag{2}$$

where t is the injection time, $p_g(t)$ is the grouting pressure at the injection hole, dt is the time step, and n is the number of time steps which will be introduced in the following section.

Furthermore, the relative grouting efficiency (RGE) is introduced to analyze the influences of the operation parameter adjustment schemes on the grouting process. The RGE is defined as the ratio of the GE of the grouting process with adjusted parameters to that of the process with constant grouting parameters and can be expressed as follows:

$$RGE = \frac{GE_{adjust}}{GE_{const}}, \tag{3}$$

where RGE is the relative grouting efficiency, GE_{adjust} is the GE under the grouting condition of the adjustment pressure, and GE_{const} is the GE calculated under the constant boundary condition. As the RGE is calculated, the total mechanical energy consumed in different grouting processes is considered the same, regardless of the boundary condition of the pressure grouting or the flow rate grouting at the injection borehole. According to Eqs. (1) and (2), the constant grouting pressure could be determined to be equal to the average at the injection hole during a special time interval.

According to the theory of the iterative method, the grouted zone can be divided into finite elements based on the time interval. In every time interval, the key grouting parameters, such as penetration length, grouting pressure, and flow rate, can be calculated. Figure 1 shows the stepwise calculation method under dynamic pressure conditions. The steps can be summarized as follows:

First, the initial grouting parameters such as the grouting pressure, the width of the rock fissure, radius of grouting hole, and grouting time are input. The function of slurry diffusion velocity is used to calculate the initial average velocity. Thus, the locations of the element boundaries will be determined by the velocity. Then, the pressure difference of

the element that enables the grout's flow will be determined according to the penetration length during one time step. The grouting pressure for the next element will subsequently be calculated by summing the previous pressure segments to determine the average velocity at the next element. Moreover, the flow rate can be calculated based on the conservation of mass. Finally, the above procedures will be repeated while increasing the injection time until the injection time reaches the specified value. The fundamental parameters calculated in the grouted area will be output automatically.

Laboratory test

Materials

The grout solutions selected in this research consisted of a colloidal silica suspension and an accelerator (Pedrotti et al. 2017). The accelerator was prepared by mixing 500 g of analytically pure NaCl particles with 4.5 kg of purified water. The colloidal silica grout was mixed with an accelerator at a selected mixing ratio before injection. The gel time of the silica sol was controlled by varying the amount of accelerator added to the colloidal silica suspension; the higher the concentration of the saline solution, the faster is the gelling (Agapoulaki and Papadimitriou 2018).

Colloidal silica contains approximately 40% silica solids by weight. An NDJ-9S rotational viscometer was used to measure the dynamic viscosity of the colloidal silica solutions under room temperature conditions. The colloidal silica suspension before the addition of the accelerator had a pH of 9.3, a density of 1290 kg/m^3, and a dynamic viscosity of 26 mPa s. The accelerator, which had a density of 1150 kg/m^3 and a neutral pH of 7, had a dynamic viscosity of 1.10 mPa s. The properties of the selected grout, a mixture of the colloidal silica and saline solution, in this laboratory test are listed in Table 1.

Figure 2a presents the viscosity versus time curves of the silica sol with three different mixing ratios. This figure shows that all colloidal silica grouts exhibit high viscosity over time. There is no observable change in the slurry viscosity when the mixing time is less than the gel induction time, at which time the viscosity has doubled and reaches approximately 16 mPa s. The value increases more rapidly with further increases in time. According to the growth rate, the injection time can be divided into three stages: the constant viscosity period extending from the starting time to the gel induction time, the slow-speed growth period in which the viscosity increases to approximately 100 mPa s, and the high-speed growth period in which the viscosity increases rapidly to a few thousand mPa s, leading to gelation.

According to Wei et al. (2019), the adjustment of operation parameters can significantly affect the fracture
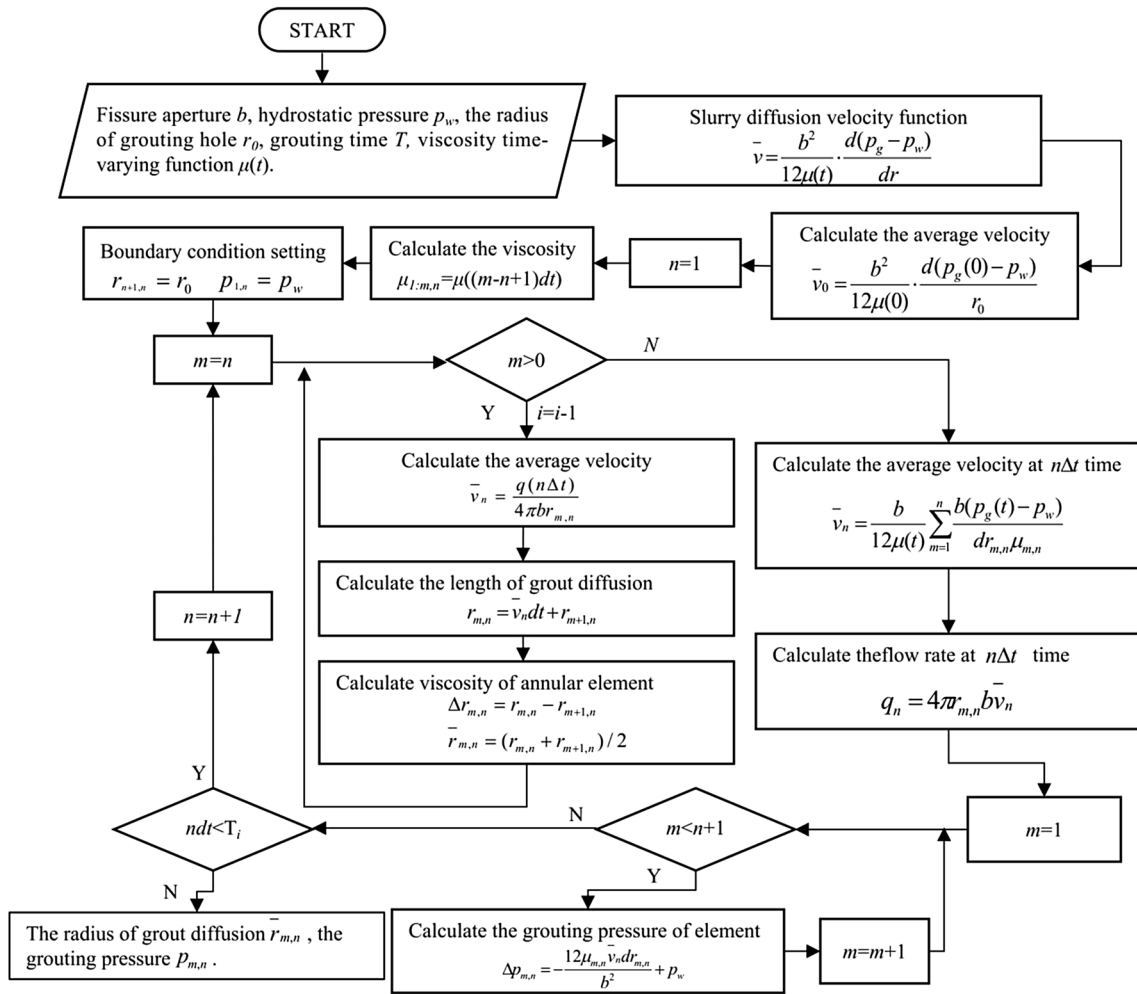
Fig. 1 Procedure of the stepwise calculation program corresponding to the parameter-adjusted grouting process (modified from Wei et al. 2019)

Table 1 Properties of grouting materials selected in the laboratory test

Grout recipes	Mixing ratio		Temp	Density ρ (kg/m^3)	Initial viscosity, μ_0 (mPa s)	Slurry viscosity function of injection time, $\mu(t)$
	40% Colloidal silica	10% NaCl solution				
G1	7	1	25.2–25.8	1225–1230	40 ± 2	$ct^3 + dt^2 + et + \mu_0$
G2					170 ± 2	$\mu_0 * \exp(ft)$

propagation, especially for slurries with remarkable rheological properties. Therefore, the silica sol in the slow-speed growth stage and high-speed growth stage was selected in this study, representing slurries with different rheological properties. The two kinds of grout were referred to as G1 and G2, with a special initial viscosity of approximately 40 mPa s and 170 mPa s, respectively. The dynamic viscosity curves in Fig. 2b were fitted by a multivariate function and an exponential function, and

the viscosity function of the injection time (timing with a special initial viscosity) was established as follows:

G1:

$$\mu(t) = ct^3 + dt^2 + et + 40 \pm 2 \text{ mPa s}, \tag{4}$$

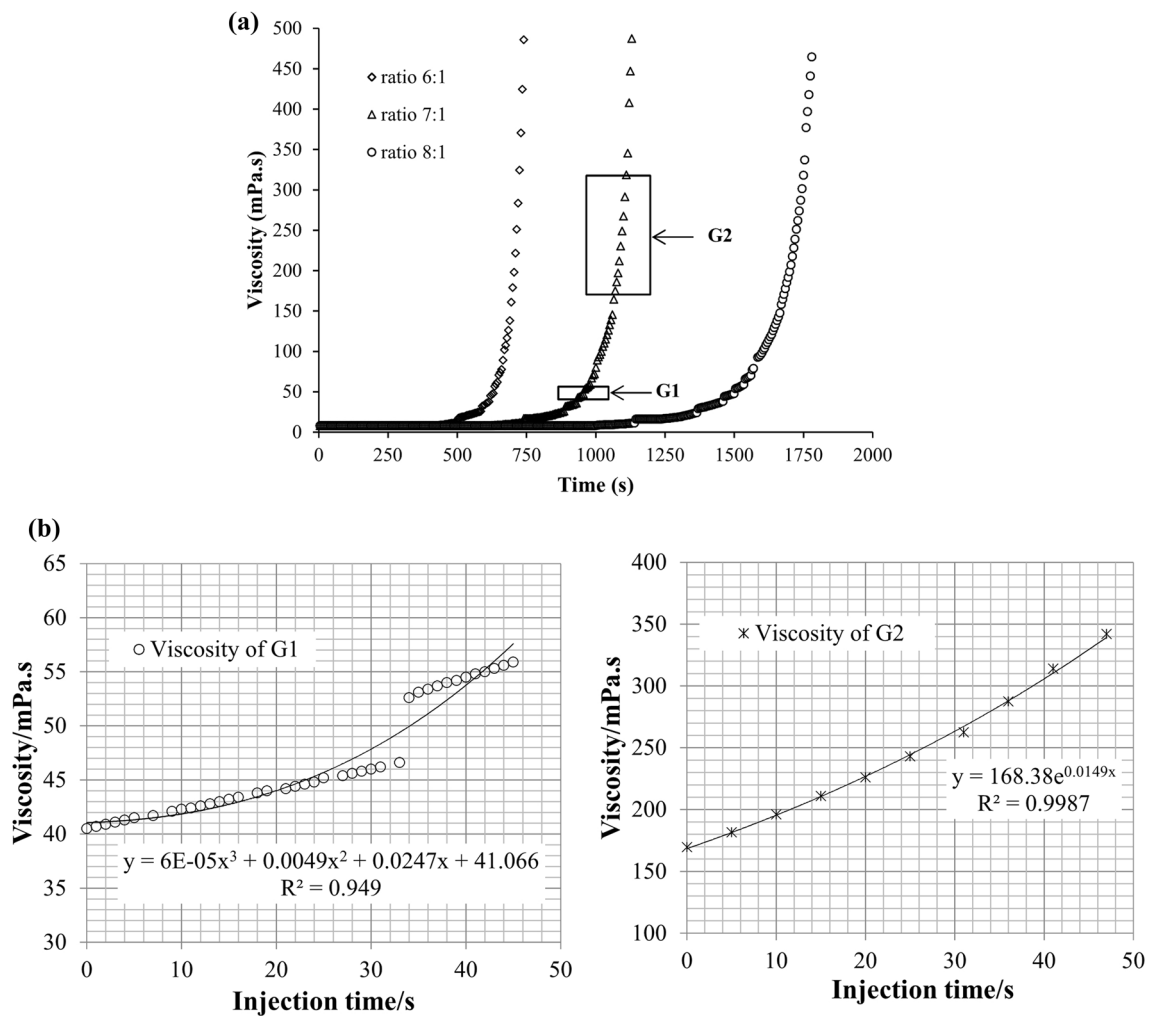G2:

$$\mu(t) = (170 \pm 2)\exp(ft) \text{ mPa s}, \tag{5}$$

Fig. 2 Mixing ratio influence on colloidal silica properties. **a** Grout viscosity with time after addition of accelerator. **b** Viscosity change of selected grouts over time, for example, left for trial no. 3–1 and right for trial no. 3–2, a trend line is fitted

where *c, d, e,* and *f* are data fitting coefficients varying in each trial.

However, a series of viscosity tests show that even two groups of grout with the same test conditions, such as the mixing ratio, mixing time, instrument speed and room temperature, will not share a qualitatively similar viscosity versus time curve. To ensure that the change curves of the viscosity were as consistent as possible, the following method was adopted in the experimental investigation. An adequate 10% NaCl solution was prepared to meet the need for all of the trials prior to the start of the research. For each trial, the mixture of silica sol and saline solution was divided into two parts. One part was used to identify the dynamic viscosity varying with time. The other part was used for the experiment. According to the above procedures, the viscosity changes in the two parts of the grout can be considered

synchronous. When the tested viscosity reached the special initial value, the trial started immediately.

In terms of one batch of prepared grout, two sequence trials could be carried out, in which the special initial viscosity was set to 40 ± 2 mPa s and 170 ± 2 mPa s. A series of preliminary experiments demonstrated that the time interval between the two initial values was approximately 3 min, which consequently determined the time interval between the two sequences of the trial.

Experimental setup

The experimental setup for investigating dynamic pressure grouting in an artificial fracture is shown in Fig. 3.

Two smooth rectangular stiff plexiglass discs with thicknesses of 10 mm were employed in this study to simulate a
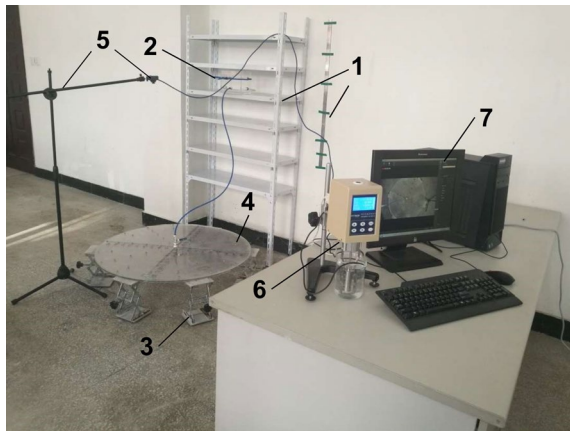
Fig. 3 Grouting system setup with all components. 1—adjustment pressure difference system; 2—grout tank; 3—lifting platform; 4—transparent fracture replica; 5—high-speed camera; 6—rotational viscometer; 7—PC

rock fracture. The strength and friction properties of stiff plexiglass are suitable for the simulation of the characteristics of rock fractures. The discs were fastened together using 56 bolts. The maximum grouting pressure of 0.8 MPa was significantly smaller than the tension stress of the bolt, and the negative effect of expansion of the aperture was neglected. The fracture space ranged from 0.2 to 1.0 mm and was adjusted by placing shims with precise thicknesses. The parallel plate had a diameter of 0.5 m. The grouting hole (diameter = 10 mm) was drilled at the center of the lower disc. Six lifting platforms were placed at the bottom of the experimental setup to adjust the level of the fracture replica.

The silica sol was poured into a cubic plexiglass tank with a side length of 150 mm. The tank was connected to the injection hole of the parallel plane fracture through a tube. During the grouting process, phasic variation of the grouting pressure was induced by moving the tank to the corresponding height on the grouting platform. Due to the limitation of the size of the artificial parallel plane fracture, the pressure injection experiments were carried out with low grouting pressure, and the maximum head difference between the fracture replica and the fluid level was set to 150 cm.

In addition, a high-speed camera connected to a computer was employed to film the entire grouting test, and the video was used to analyze the slurry diffusion in the fracture replica.

Design of the experiments

Grouting efficiency is affected by many factors, such as the characteristics of the structural plane, grouting modes, and rheological properties of the grout (Sui et al. 2015; Wei et al. 2019). In this experiment, it is difficult to consider all the factors in a limited number of tests. Therefore, several main factors, including the grout viscosity, the fracture aperture width, and the stage change schemes of grouting pressure, were used in this study.

Tables 2 and 3 list the arrays of a total of 40 experiments with four factors, such as the hydraulic aperture, slurry type, adjustment schemes of pressure head difference, and injection time. The hydraulic aperture (200 μm and 250 μm selected for this study) could be computed using the "cubic law", which was introduced in detail by Funehag and Thörn (2018). Three dynamic pressure head difference schemes were adopted in this investigation, including the constant pressure, phased increased pressure and phased reduced pressure. For constant pressure grouting, the pressure head difference, i.e., the vertical distance between the fluid level in the grout tank and the fracture replica, is maintained at 90 cm and 110 cm, respectively. In addition, four schemes, 70–90–100, 50–90–130, 90–110–130 and 70–110–150, were adopted in the phased increased pressure grouting scheme. However, four inverse adjustment schemes for the pressure head difference were used in the phased reduced pressure grouting, namely 110–90–70, 130–90–50, 130–110–90, and 150–110–70. In terms of each grouting pressure scheme, the location and the value of the number represented the step number and the grouting pressure for a trial. For example, 70–90–100 means that a trial consists of three steps, each of which corresponds to a pressure head difference of 70, 90 and 110 cm, respectively. Furthermore, the total grouting time for any trial was set at 45 s, that is, the grouting time allocated for each step was 15 s, denoted as 15–15–15.

Prior to each test, the high-speed camera was turned to ensure that the entire trial was filmed, and the level of the transparent fracture replica was set using the lifting platform. The mixture of silica sol and saline solution was poured into the grout tank. Once the viscosity of the mixture approached the specified viscosity, the timer was started, and the valve was opened to allow injection of the grout into the fracture. During the grouting experiment, variation of the injection pressure was achieved by moving the tank to the corresponding height on the grouting platform. The pressure was determined according to Eq. 6.

$$p_g = \rho g h, \tag{6}$$

where ρ is the density of the mixture of silica sol and saline solution, which was measured in every test, p_g is the grouting pressure, g is the acceleration of gravity, and h is the vertical height from the fracture replica to the grout fluid surface.

At the end of each trial, the fractured replica was washed with pressurized water and compressed air for approximately 2 min, and the injected silica sol slurry was completely discharged from the fracture replica.

Table 2 Experimental and theoretical results for grouting in a fracture with an aperture width of 200 μm

Trial no.	Slurry selected	Pressure head difference, ΔH (cm)	Injection time, t (s)	Radius of separation (m)			Relative grouting efficiency		Differences ratio (%)	
				I_{cal}	I^*_{cal}	I_{exp}	RGE_{cal}	RGE_{exp}	β_I	β_{RGE}
1–1	G1	70–90–110	15–15–15	0.16	0.161	0.159	0.994	0.994	− 0.6	0
2–1		50–90–130	15–15–15	0.161	0.163	0.154	0.988	0.963	− 4.3	− 2.5
3–1		90–90–90	15–15–15	0.164	0.164	0.16	1	1	− 2.4	0
4–1		110–90–70	15–15–15	0.162	0.159	0.163	1.019	1.019	0.6	0
5–1		130–90–50	15–15–15	0.163	0.159	0.166	1.025	1.038	1.8	1.3
6–1		90–110–130	15–15–15	0.172	0.173	0.168	0.994	0.918	− 2.3	− 7.6
7–1		70–110–150	15–15–15	0.174	0.176	0.17	0.989	0.929	− 2.3	− 6.1
8–1		110–110–110	15–15–15	0.178	0.178	0.183	1	1	2.8	0
9–1		130–110–90	15–15–15	0.181	0.179	0.187	1.011	1.022	3.3	1.1
10–1		150–110–70	15–15–15	0.17	0.167	0.178	1.018	0.973	4.7	− 4.4
1–2	G2	70–90–110	15–15–15	0.076	0.077	0.069	0.987	0.896	− 9.2	− 9.2
2–2		50–90–130	15–15–15	0.074	0.077	0.065	0.961	0.844	− 12.2	− 12.2
3–2		90–90–90	15–15–15	0.075	0.075	0.077	1	1	2.7	0
4–2		110–90–70	15–15–15	0.076	0.075	0.08	1.013	1.039	5.3	2.6
5–2		130–90–50	15–15–15	0.077	0.075	0.082	1.027	1.065	6.5	3.7
6–2		90–110–130	15–15–15	0.084	0.085	0.082	0.988	0.965	− 2.4	− 2.3
7–2		70–110–150	15–15–15	0.083	0.084	0.076	0.988	0.894	− 8.4	− 9.5
8–2		110–110–110	15–15–15	0.084	0.084	0.085	1	1	1.2	0
9–2		130–110–90	15–15–15	0.085	0.084	0.094	1.012	1.106	10.6	9.3
10–2		150–110–70	15–15–15	0.087	0.085	0.096	1.024	1.129	10.3	10.3

Table 3 Experimental and theoretical results for grouting in a fracture with an aperture width of 250 μm

Trial no.	Slurry selected	Pressure head difference, ΔH (cm)	Injection time, t (s)	Radius of separation (m)			Relative grouting efficiency		Differences ratio (%)	
				I_{cal}	I^*_{cal}	I_{exp}	RGE_{cal}	RGE_{exp}	β_I	β_{RGE}
11–1	G1	70–90–110	15–15–15	0.192	0.194	0.187	0.99	0.964	− 2.6	− 2.6
12–1		50–90–130	15–15–15	0.194	0.195	0.19	0.995	0.979	− 2.1	− 1.6
13–1		90–90–90	15–15–15	0.195	0.195	0.194	1	1	− 0.5	0
14–1		110–90–70	15–15–15	0.192	0.189	0.195	1.016	1.005	1.6	− 1.1
15–1		130–90–50	15–15–15	0.196	0.19	0.197	1.032	1.015	0.5	− 1.6
16–1		90–110–130	15–15–15	0.215	0.219	0.212	0.982	0.942	− 1.4	− 4.1
17–1		70–110–150	15–15–15	0.21	0.222	0.22	0.946	0.978	4.8	3.4
18–1		110–110–110	15–15–15	0.206	0.206	0.225	1	1	9.2	0
19–1		130–110–90	15–15–15	0.235	0.222	0.243	1.059	1.08	3.4	2
20–1		150–110–70	15–15–15	0.245	0.227	0.248	1.079	1.102	1.2	2.1
11–2	G2	70–90–110	15–15–15	0.091	0.093	0.083	0.978	0.856	− 8.8	− 12.5
12–2		50–90–130	15–15–15	0.089	0.091	0.084	0.978	0.866	− 5.6	− 11.5
13–2		90–90–90	15–15–15	0.093	0.093	0.097	1	1	4.3	0
14–2		110–90–70	15–15–15	0.094	0.093	0.105	1.011	1.082	11.7	7
15–2		130–90–50	15–15–15	0.093	0.093	0.103	1	1.062	10.8	6.2
16–2		90–110–130	15–15–15	0.1	0.101	0.092	0.99	0.958	− 8	− 3.2
17–2		70–110–150	15–15–15	0.097	0.099	0.087	0.98	0.906	− 10.3	− 7.6
18–2		110–110–110	15–15–15	0.1	0.1	0.096	1	1	− 4	0
19–2		130–110–90	15–15–15	0.1	0.097	0.113	1.031	1.177	13	14.2
20–2		150–110–70	15–15–15	0.103	0.101	0.11	1.02	1.146	6.8	12.4

Results of the tests

Grouting process

A high-speed camera was used to film the grout dispersion in each trial. The diffusion radius of the experiments could be interpreted from the captured video at an interval of 3 s. The video is captured in real time, and at each time step the video is paused and a photo is derived. The penetration length at any time is the average value of the intercepts with the x-axis and y-axis.

The results are listed in Tables 2 and 3. In these tables, I_{exp} is the actual radius of the dispersion at the end of the injection time (45 s), I_{cal} is the radius calculated based on the measured slurry viscosity and grouting pressure, and I^*_{cal} is the predicted radius obtained by using the measured viscosity and the calculated constant grouting pressure

for each trial. Note that, in these predicted results, the measured adjustment grouting pressure is obtained using Eq. 6, and the calculated constant pressure is the average of changing the injection pressure of three stages in one experiment. The viscosity function of the injection time is established in every trial according to Eqs. 4 and 5. Moreover, β_I and β_{RGE} represent the difference ratio between the actual values and predicted values for the radius of separation and relative grouting efficiency, respectively.

The results indicate that the theoretical model gave somewhat faster grout flow than the actual results for the grouts with a slow-growth viscosity (i.e., G1); however, the reverse is true for the grouts with a rapid-growth viscosity (i.e., G2). In addition, the actual penetration length is much larger than the theoretical data under the phased reducing pressure condition. In principle, however, there was good agreement between the predicted calculations
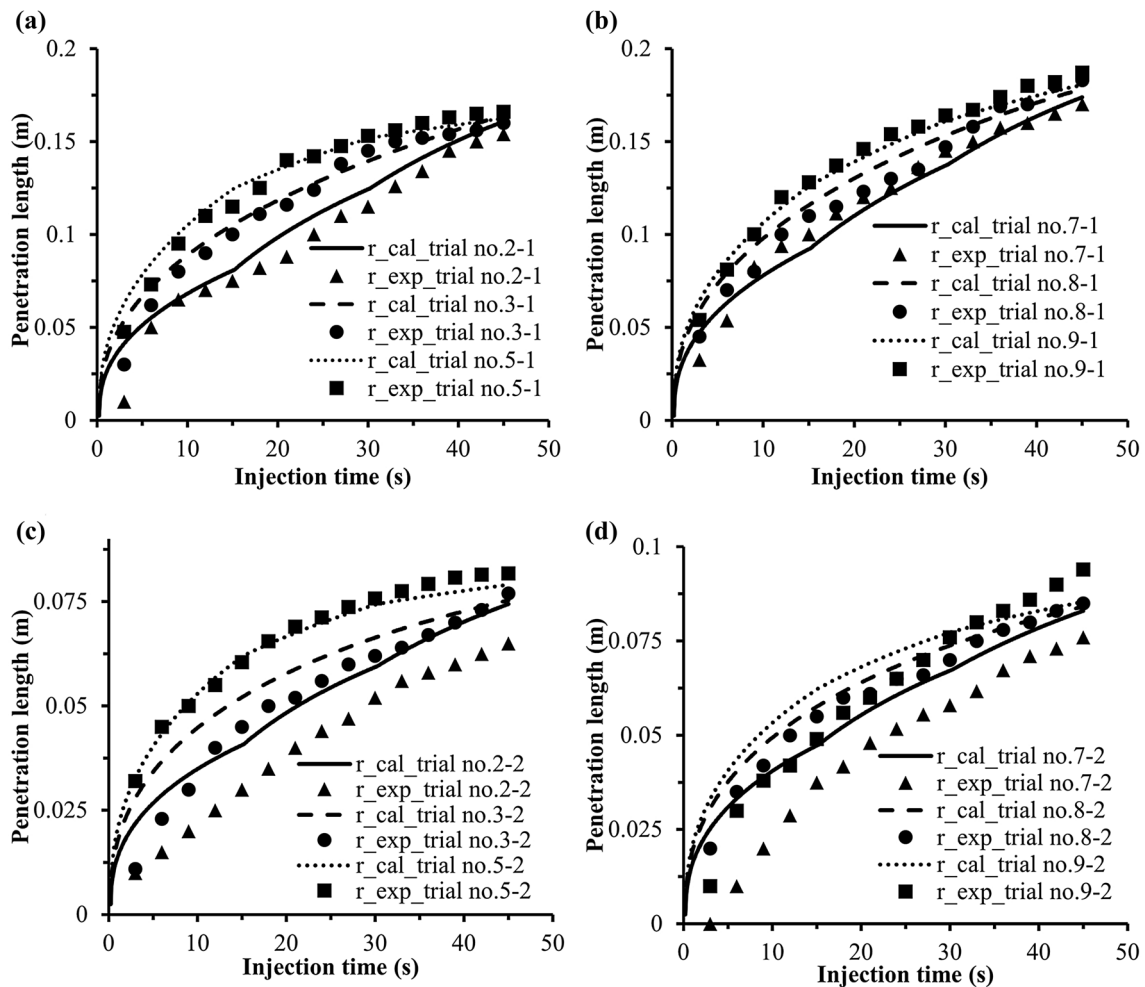

Fig. 4 Actual and theoretically predicted propagation under dynamic pressure adjustment condition in the fracture with aperture width 200 μm. **a** Average pressure difference of 90 cm for grout G1, **b** average pressure difference of 110 cm for grout G1, **c** average pressure difference of 90 cm for grout G2 and **d** average pressure difference of 110 cm for grout G2

based on the stepwise method and the actual values, especially for the weak rheological grout G1.

Both the actual and theoretical propagation results as a function of time are depicted in Figs. 4 and 5.

The theoretical penetration lengths are calculated based on the modified stepwise algorithm proposed by Wei et al. (2019), and the time-varying function of slurry viscosity required in the calculation process is obtained by fitting the measured data using a rotational viscometer. As shown in Figs. 4 and 5, the actual penetration lengths agreed fairly well with the theoretical calculations, especially for grout G1.

In addition, three grouting processes involved in each diagram consume equal mechanical energy, but the corresponding penetration length versus time curves show a different trend. Under the condition of constant pressure grouting, the penetration length increases with increasing grouting durability time, and the penetration rate declines

due to the decreasing flow rate and radial flow manner. As the grouting pressure increases or decreases step by step, the grout propagation tendency shows observable phase change characteristics. In each stage, the penetration rate undergoes a gradual reducing process. However, as the slurry viscosity increases over time, this tendency becomes unclear. Under the above three grouting pressure adjustment conditions, the maximum penetration length produced by periodic-reducing pressure, constant pressure, and periodic-increasing pressure decreases successively, which is verified by both the theoretical and measured results.

Grouting efficiency

The theoretical and experimental RGE was calculated according to Eq. (3). The theoretical value of RGE is defined as the ratio of the theoretical GE for each trial to that of the
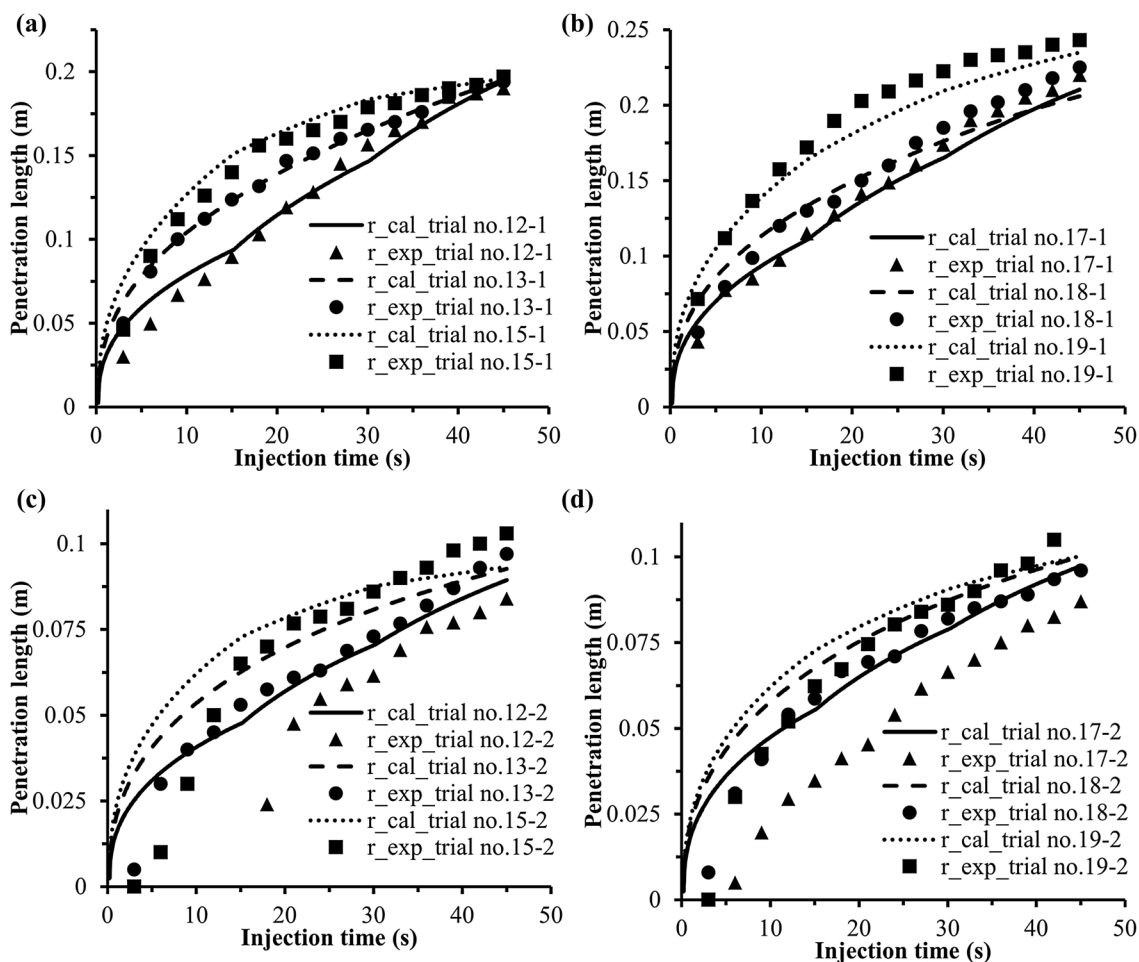

Fig. 5 Actual and theoretically predicted propagation under dynamic pressure adjustment condition in the fracture with aperture width 250 μm. **a** Average pressure difference of 90 cm for grout G1, **b** aver-age pressure difference of 110 cm for grout G1, **c** average pressure difference of 90 cm for grout G2 and **d** average pressure difference of 110 cm for grout G2

corresponding constant pressure grouting test. Since pressure grouting is the objective in this paper, the mechanical energy consumption under dynamic pressure grouting is equal to the corresponding constant pressure grouting. Notably, the variation in the slurry viscosity used in each trial cannot be completely synchronized, resulting in slight differences in the theoretically predicted propagation distance. Similarly, the measured RGE is obtained by dividing the actual maximum diffusion distance of each grouting test by the result of the corresponding constant pressure grouting test.

Tables 2 and 3 list the RGE and difference ratios for the hydraulic apertures of 200 µm and 250 µm, respectively. The experimental data were consistent with the theoretical results, especially for the low-speed growth viscosity grout G1. The comparison between the calculated and experimental RGE values for a hydraulic aperture of 200 µm, as shown in Fig. 6, indicates that the pressure adjustment scheme has a profound impact on the GE. The RGE of phased increased pressure schemes is lower than 1, while the RGE of the phased decreased pressure schemes is greater than 1. Furthermore, the change stage of the slurry viscosity also has an obvious influence. When the slurry grout is at a relevant

lower viscosity period, the RGE of the phased increased pressure grouting ranges from 0.918 to 0.994, while the values of the phased reduced pressure varies from 0.973 to 1.038. However, as the grout with high-growth viscosity is adopted, the RGE deviates significantly from 1, and the value range is 0.844–0.965 and 1.039–1.129 for the phased increased pressure grouting and the phased reduced pressure grouting, respectively.

The comparison between the calculated and experimental RGE values for a hydraulic aperture of 250 µm is illustrated in Fig. 7. The effects of the adjustment schemes on the RGE showed a similar trend. In terms of the silica sol in the low-speed growth viscosity stage, the influence of variable pressure grouting on the GE could be ignored. For the silica sol with high-speed growth viscosity, the phased increased pressure grouting results in a 4.2–14.4% reduction in the GE compared with constant pressure grouting, while the GE could be increased by 6.2~17.7% when selecting the staged reduction pressure scheme.
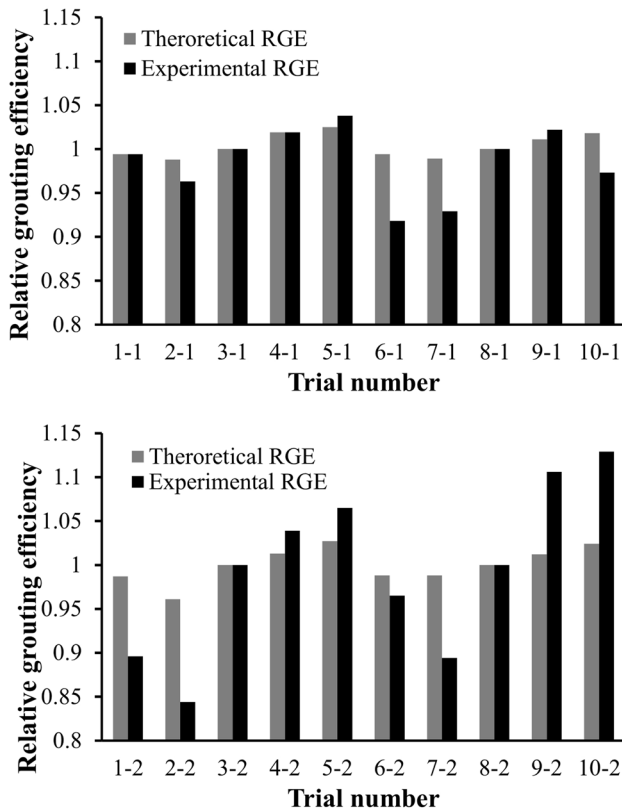

Fig. 6 Actual and theoretical relevant grouting efficiency in a fracture with an aperture width of 200 µm: upper diagram for grout G1 and lower diagram for grout G2
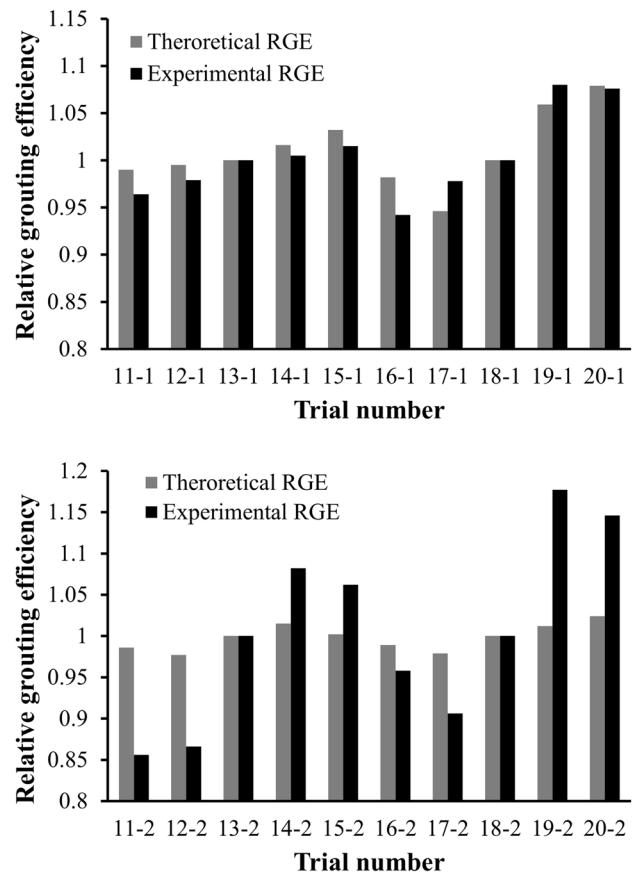

Fig. 7 Actual and theoretical relevant grouting efficiency in a fracture with an aperture width of 250 µm: upper diagram for grout G1 and lower diagram for grout G2

Discussion

This study is not intended for a specific engineering case, but mainly discusses the effect of the adjustment of the grouting pressure at the injection hole on the fracture GE. In the analysis, two issues are emphatically discussed: one issue is to obtain the maximum slurry diffusion range while consuming the same mechanical energy during the pressure grouting process; and the other issue is to obtain access to improve the fracture GE for typical grouts with varying rheology.

A series of experiments revealed that a change in the injection pressure during a grouting process can affect the fracture GE absolutely. Generally, the GE under phased increasing pressure conditions is lower than that under constant pressure grouting. Moreover, phased decreased pressure grouting can significantly improve the GE, especially for slurries with high-speed growth viscosity.

The study of GE is of profound significance for grouting design. The dynamic adjustment of the grouting pressure can allow the penetration region to meet the design value while avoiding the surrounding rock bearing high grouting pressure during the entire injection process. In addition, a reasonable adjustment of the grouting pressure can effectively promote grout propagation, especially for fractures with a narrow aperture.

In engineering practice, most grouting materials, such as cement–sodium silicate paste and silica sol, exhibit different rheological properties, which are characterized by a phased variation. In terms of grouts with different rheological stages, suitable pressure adjustment schemes should be selected. When the viscosity of the grout remains at a constant period or low-speed growth stage, constant pressure or phased increased pressure grouting can be considered. Nevertheless, phased reduced pressure grouting should be chosen as the viscosity of the grout enters a high-speed growth period to increase the grout penetration length.

Conclusions

A series of experiments were performed for typical grouts with time-dependent viscosity into a fracture under a phased changed injection pressure using a grouting system with a transparent fracture replica. A total of three major influencing factors on the fracture GE were taken into consideration in the experiments: the rheological property of the grout, adjustment scheme of injection pressure, and hydraulic aperture. The analysis of the experimental results indicates that the pressure adjustment mode is a deterministic factor for the deviation of the fracture GE (i.e., improvement or reduction in the GE); moreover, the change degree is dominated by the rheological property of the selected grout to a certain extent.

However, for microfissures, the influence of the hydraulic fissure width of GE could be negligible.

Comparatively, in terms of a grouting process that consumes an equal total mechanical energy, the slightest penetration length can be generated under periodic-increasing pressure conditions, whereas the maximum value can be obtained by a step-by-step reduction in the injection pressure. For the grout with slow-growth viscosity, G1, the change degree of the GE produced by the phased variation pressure is approximately 3.67%, while for the grout with rapid-growth viscosity, G2, the value increases to more than 10%. Consequently, higher grouting pressure should be applied according to the limitation of the grouting pump during the earlier grouting period. In this stage, the selected slurry is characterized by relatively low viscosity and high fluidity; moreover, higher grouting pressures could promote the effective dispersion of the slurry in a fracture. However, it should be noted that the hydraulic fracturing of the surrounding rock mass should be avoided by the applied grouting pressure. In addition, the result indicates that the measured penetration length versus injection time curves agree well with the theoretical values.

References

Agapoulaki GI, Papadimitriou AG (2018) Rheological properties of colloidal silica grout for passive stabilization against liquefaction. J Mater Civil Eng 30(10):04018251

Amadei B, Savage WZ (2001) An analytical solution for transient flow of Bingham viscoplastic materials in rock fractures. Int J Rock Mech Min Sci 38(2):285–296

Axelsson M, Gustafson G, Fransson Å (2009) Stop mechanism for cementitious grouts at different water-to-cement ratios. Tunn Undergr Sp Tech 24(4):390–397

Cheng JL, Sun XY, Zheng G, Gao F, Kong XR, Zhou J (2013) Numerical simulations of water-inrush induced by fault activation during deep coal mining based on fluid-solid coupling interaction. Disaster Adv 6(11):10–14

Dai G, Bird RB (1981) Radial flow of a Bingham fluid between two fixed circular disks. J Non-newton Fluid Mech 8(3):349–355

Funehag J, Fransson A (2006) Sealing narrow fractures with a Newtonian fluid: model prediction for grouting verified by field study. Tunn Undergr Sp Tech 21(5):492–498

Funehag J, Gustafson G (2008a) Design of grouting with silica sol in hard rock—new methods for calculation of penetration length, part I. Tunn Undergr Sp Tech 23(1):1–8

Funehag J, Gustafson G (2008b) Design of grouting with silica sol in hard rock—new design criteria tested in the field, part II. Tunn Undergr Sp Tech 23(1):9–17

Funehag J, Thorn J (2018) Radial penetration of cementitious grout: Laboratory verification of grout spread in a fracture model. Tunn Undergr Sp Tech 72(2018):228–232

Guo WJ, Wang HL, Chen SJ (2016) Coal pillar safety and surface deformation characteristics of wide strip pillar mining in deep mine. Arab J Geosci 9(2):137

Guo WJ, Zhao JH, Yin LM, Kong DZ (2017) Simulating research on pressure distribution of floor pore water based on fluid-solid coupling. Arab J Geosci 10(1):5

Gustafson G, Stille H (1996) Prediction of groutability from grout properties and hydrogeological data. Tunn Undergr Sp Tech 11(3):325–332

Hassler L, Hakansson U, Stille H (1992) Computer-simulated flow of grouts in jointed rock. Tunn Undergr Sp Tech 7(4):441–446

Huang WP, Li C, Zhang LW, Yuan Q, Zheng YS, Liu Y (2018) In situ identification of water-permeable fractured zone in overlying composite strata. Int J Rock Mech Min 105:85–97

Li SC, Han WW, Zhang QS, Liu RT, Weng XJ (2013) Research on time-dependent behavior of viscosity of fast curing grouts in underground construction grouting. Chin J Rock Mech Eng 32(1):1–7 **(in Chinese)**

Li SC, Zhang WJ, Zhang QS, Zhang X, Liu RT, Pan GM, Li ZP, Che ZY (2014) Research on advantage-fracture grouting mechanism and controlled grouting method in water-rich fault zone. Chin J Rock Mech Eng 35(3):744–752 **(in Chinese)**

Li LY, Wei JC, Yin HY, Xie J, Ding YS, Shi SQ (2018a) Influence of sedimentary facies on reservoir quality and distribution of diagenetic features in the Funing Formation, Wanglongzhuang Oilfield, Subei Basin, Eastern China. Arab J Geosci 11(15):432

Li ZX, Wang DD, Lv DW, Li Y, Liu HY, Wang PL, Liu Y, Liu JQ, Li DD (2018b) The geologic settings of Chinese coal deposits. Int Geol Rev 60(5–6):548–578

Li H, Bai HB, Wu JJ, Meng QB, Ma K, Wu LY, Meng FF, Wang SJ (2019a) A Set of Methods to Predict Water Inrush from an Ordovician Karst Aquifer: a case study from the Chengzhuang Mine. China Mine Water Environ 38(1):39–48

Li WT, Yang N, Mei YC, Zhang YH, Wang L, Ma HY (2019b) Experimental investigation of the compression-bending property of the casing joints in a concrete filled steel tubular supporting arch for tunnel engineering. Tunn Undergr Sp Tech. https://doi.org/10.1016/j.tust.2019.103184

Littlejohn GS (1975) Acceptable water flows for rock anchor grouting. Ground Eng 8(2):46–48

Lu YL, Wang LG (2015) Numerical simulation of mining-induced fracture evolution and water flow in coal seam floor above a confined aquifer. Comput Geotech 67:157–171

Mohajerani S, Baghbanan A, Bagherpour R, Hashemolhosseini H (2015) Grout penetration in fractured rock mass using a new developed explicit algorithm. Int J Rock Mech Min Sci 80:412–417

Mohammed MH, Pusch R, Knutsson S (2015) Study of cement-grout penetration into fractures under static and oscillatory conditions. Tunn Undergr Sp Tech 45:10–19

Pedrotti M, Wong C, El Mountassir G, Lunn RJ (2017) An analytical model for the control of silica grout penetration in natural groundwater systems. Tunn Undergr Sp Tech 70:105–113

Shi SQ, Wei JC, Xie DL, Yin HY, Li LY (2019) Prediction analysis model for groundwater potential based on set pair analysis of a confined aquifer overlying a mining area. Arab J Geosci 12(4):115

Sui WH, Liu JY, Hu W, Qi JF, Zhan KY (2015) Experimental investigation on sealing efficiency of chemical grouting in rock fracture with flowing water. Tunn Undergr Sp Tech 50(1):239–249

Sun WJ, Wu Q, Liu HL, Jiao J (2015) Prediction and assessment of the disturbances of the coal mining in Kailuan to karst groundwater system. Phys Chem Earth Parts A/B/C 89–90:136–144

Sun ZZ, Yan X, Liu RT, Xu ZH, Li SC, Zhang YM (2018) Transient analysis of grout penetration with time-dependent viscosity Inside 3D fractured rock mass by unified pipe-network method. Water 10(9):1122

Tan YL, Ning JG, Li HT (2012) In situ explorations on zonal disintegration of roof strata in deep coalmines. Int J Rock Mech Min Sci 49:113–124

Tan YL, Zhao TB, Xiao YX (2010) In situ investigations of failure zone of floor strata in mining close distance coal seams. Int J Rock Mech Min 47(5):865–870

Wang DD, Shi LQ (2019) Source identification of mine water inrush: a discussion on the application of hydrochemical method. Arab J Geosci 12(2):58

Wang G, Han W, Jiang YJ, Luan HJ, Wang K (2019) Coupling analysis for rock mass supported with CMC or CFC rockbolts based on viscoelastic method. Rock Mech Rock Eng 52:4565–4588

Wang G, Wu MM, Wang R, Xu H, Song X (2017) Height of the mining-induced fractured zone above a coal face. Eng Geol 216:140–152

Wang X, Meng FB (2018) Statistical analysis of large accidents in China's coal mines in 2016. Nat Hazards 92(1):311–325

Wei JC, Han CH, Zhang WJ, Xie C, Zhang LZ, Li XP, Zhang CR, Jiang JG (2019) Mechanism of fissure grouting based on step-wise calculation method. Rock and Soil Mech 40(3):913–925 **(in Chinese)**

Wu Q, Liu YZ, Liu DH, Zhou WF (2011) Prediction of floor water inrush: the application of GIS-based AHP vulnerable index method to Donghuantuo Coal Mine. China Rock Mech Rock Eng 44(5):591–600

Yao QL, Li XH, Zhou J, Qu QD, Cao SG (2013) Technology of coal seam floor grouting for disaster prevention and control while mining above a confined water body. Disaster Adv 6:216–227

Yin HY, Wei JC, Lefticariu L, Guo JB, Xie DL, Li ZL, Zhao P (2016) Numerical simulation of water flow from the coal seam floor in a deep longwall mine in china. Mine Water Environ 35(2):1–10

Yin HY, Zhao H, Xie DL, Sang SZ, Shi YL, Tian MH (2019) Mechanism of mine water inrush from overlying porous aquifer in Quaternary: a case study in Xinhe Coal Mine of Shandong Province. Arab J Geosci 12(5):163

Yin HY, Zhou WF, LaMoreaux JW (2018) Water inrush conceptual site models for coal mines of China. Environ Earth Sci 77:746

Yu B, Zhao J, Xiao HT (2017) Case study on overburden fracturing during longwall top coal caving using microseismic monitoring. Rock Mech Rock Eng 50(2):507–511

Zhang SC, Guo WJ, Li YY (2017a) Experimental simulation of water-inrush disaster from the floor of mine and its mechanism investigation. Arab J Geosci 10(22):503

Zhang QS, Zhang LZ, Liu RT, Li SC, Zhang QQ (2017b) Grouting mechanism of quick setting slurry in rock fissure with consideration of viscosity variation with space. Tunn Undergr Sp Tech 70:262–273

Zhang WJ, Li SC, Wei JC, Zhang QS, Liu RT, Zhang X, Yin HY (2018) Grouting rock fractures with cement and sodium silicate grout. Carbonate Evaporite 33(2):211–222

Zeng YF, Wu Q, Liu SQ, Zhai YL, Zhang W, Liu YZ (2016) Vulnerability assessment of water bursting from Ordovician limestone into coal mines of China. Environ Earth Sci 75:1431